Aeroacoustics Conferences
20-23 May 2019, Delft, The Netherlands
25th AIAA/CEAS Aeroacoustics Conference

10.2514/6.2019-2690

A Two-Dimensional Model of Sound Transmission Through Curved and Staggered OGV: Effect of Inter-Vane Channel Mode Transitions

Léo Girier [1,2] *, Michel Roger [1] †,
Hadrien Bériot [3] ‡, Anthony Lafitte [2] §, Hélène Posson [2] ¶

[1] *Laboratoire de Mécanique des Fluides et d'Acoustique*
UMR CNRS 5509, École Centrale de Lyon, Université de Lyon, 69134 Écully Cedex, France

[2] *Safran Aircraft Engines, 77550 Moissy Cramayel, France*

[3] *Siemens Industry Software NV, 3001 Leuven, Belgium*

The present work extends a recent two-dimensional analytical model for sound generation and transmission in an axial-flow outlet guide vanes row, by taking into account vane camber and stagger, as well as cut-on/cut-off or cut-off/cut-on transitions of inter-vane channel modes. It is aimed at demonstrating that such transitions may have a significant role in turbomachinery aeroacoustics, typically by changing the balance of upstream and downstream scattered waves. The model is based on a mode-matching procedure and generates a uniformly valid description of the sound field. Previous implementations neglecting the vane curvature have shown significant limitations at high frequencies compared to numerical simulations performed with a finite element method code. The extension presented in this paper introduces curvature by a slowly-varying duct formalism. Comparison with numerical simulations show substantial improvements at the cost of a reasonably higher computation time.

I. Introduction

With the exponential growth of air traffic since the 1980s, International Civil Aviation Organization (ICAO) noise standards have become more and more stringent in order to limit noise annoyance for people living in the vicinity of airports. Consequently, aircraft and engine manufacturers need to maintain a constant research effort to keep reducing overall aircraft noise. In particular, with the constant increase in bypass ratio of turbofan engines, fan related noise is today one of the main lever to reduce Effective Perceived Noise Level (EPNL). In this context, the mode-matching technique described in Bouley *et al.* [1] showed promising capabilities as a tool for fan stage pre-design, especially to further understand acoustic transmission and reflection phenomena. The present work is aimed at i) developing an analytical tool based on the mode-matching technique to model acoustic transmission phenomena in a rotor-stator stage and ii) bringing a deeper understanding of sound propagation in blades row. The objective is to include as many realistic design parameters as possible in the model while preserving analytical tractability, so that fast computations are ensured especially for broadband noise. The model should also perform efficiently in an optimization strategy.

The paper focuses on the study of sound transmission through an Outlet Guide Vanes (OGV) row using a two dimensional formulation of the analytical model presented by Roger *et al.* [2]. An improvement of the model, taking into account the effect of vane camber on sound propagation, is presented in this paper.

The implementation of camber also reproduces the diffuser effect of the OGV row by the equivalent stream-wise variation of the inter-vane channel cross-section. This has a significant effect on the amplitudes and wavenumbers of the acoustic modes. In particular the mechanism known as cut-off/cut-on or cut-on/cut-off transition for inter-vane channel modes is also expected. The results shown in this paper, as a preliminary implementation, are obtained without mean flow, though including flow is not a difficulty as shown in Bouley *et al.* [1].

*PhD student, Aerodynamics and Aeroacoustics Department, leo.girier@ec-lyon.fr
†Professor
‡R&D Research Engineering Manager
§R&T Aeroacoustics Engineer, Aerodynamics and Aeroacoustics Department
¶R&T Aeroacoustics Engineer, Aerodynamics and Aeroacoustics Department

The outline of the paper is as follows. State of the art on the mode-matching technique and sound propagation in ducts of varying cross-section are presented in section II alongside the geometrical approximations used to describe the inter-vane channels. The newly added implementation of vane camber in the modified mode-matching equations is also described. Pressure fields computed with the developed algorithm are then compared with numerical simulations in section III. Finally, the influence of inter-vane channel mode transitions on the acoustic power balance is discussed in section IV.

II. Mode-Matching Technique

A. Background

The mode-matching technique is used to solve boundary value problems with linear frequency-domain differential equations. This technique is well suited when the geometry of the problem can be seen as the junction of multiple sub-regions. Such problems can arise for wave propagation in ducts with liners on specific portions of the wall or for wave scattering through bifurcated channels. In particular, sound propagation through an OGV row seen in a 2-D unwrapped cut at a constant radius can be viewed as an example of the latter case. An explanatory scheme is given in Fig. 1. An incident mode, described by its velocity potential ϕ_i, is scattered at the OGV Leading-Edge (LE) interface, generating reflected modes ϕ_r and transmitted modes ϕ_d in the channels that scatter again at the Trailing-Edge (TE) interface, giving rise to reflected channel modes ϕ_u and transmitted modes ϕ_t. Hard-walled boundary conditions at the walls of inter-vane channels and periodic boundary conditions in the y-direction are imposed. In the mode-matching

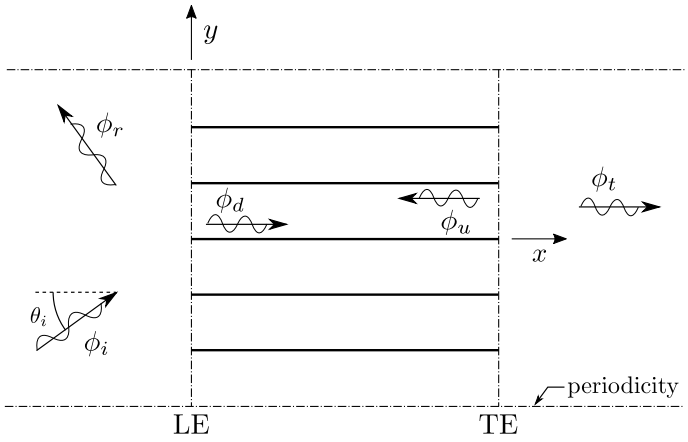

Fig. 1 Scattering of an acoustic wave through an OGV row seen in 2-D at a given radius.

technique, the Helmholtz equation is solved for all scattered potentials. The method can be described in three steps: partitioning, solving and matching. The partitioning consists in dividing the domain into different sub-domains in which the boundary conditions are uniform, allowing a solution of the Helmholtz equation on a local modal basis. In Fig. 1, the sub-domains are the upstream medium, the inter-vane channels and the downstream medium. The solving step is self-explanatory and provides the solution in each sub-domains in a modal form. Finally, the matching procedure connects the different modal solutions at both leading-edge and trailing-edge interfaces (Fig. 1). To do so, it uses continuity equations specific to the problem in order to build a set of equations on the modal coefficients that can be solved by matrix inversion.

The mode-matching technique was first used for electromagnetic fields by Whitehead [3] and the method was later described in details by Mittra and Lee [4]. In the context of cascade aeroacoustics, Bouley *et al.* [1] recently developed a mode-matching technique to study sound transmission and generation through OGV in axial-flow turbofan engines (an exhaustive list of references can also be found in the paper). Bouley *et al.* [1] used an unwrapped 2-D model at a given duct radius and modeled the vanes by infinitely thin flat plates with zero stagger, which corresponds exactly to the problem in Fig. 1 with the addition of a mean flow. The model was subsequently improved to account for stagger angle at the leading edge using Green's second identity, as described by Roger & François [5]. Roger *et al.* [2] later improved the model with a natural extension of mode-matching to make the solution of the potentials ϕ_d and ϕ_u available in the

entire inter-vane channel for any stagger. They also did a preliminary investigation on the diffuser effect of the OGV row due to an increasing inter-vane channel cross-section. This effect is introduced when vane mean camber is taken into account. To do so, vane profiles were modeled using circle arcs (see Fig. 2a). With this approximation, the sound field was only available in the domain BA'C'C. To address this problem, they slightly modified the geometry to allow the definition of acoustic modes in the triangle part of the inter-vane channels defined by the points A, A' and B in Fig. 2b. Good agreements were obtained by Roger & Moreau [6] when applying the mode-matching technique with cambered vanes compared to Hixon's [7] results with the NASA Glenn Research Center BASS code which solves the fully nonlinear Euler equations. Roger *et al.* [2] and Roger & François [5] then used Ovenden's [8] solution for the velocity potential to highlight the effect of cut-on/cut-off transition on sound propagation but did not implement this mechanism in the mode-matching technique.

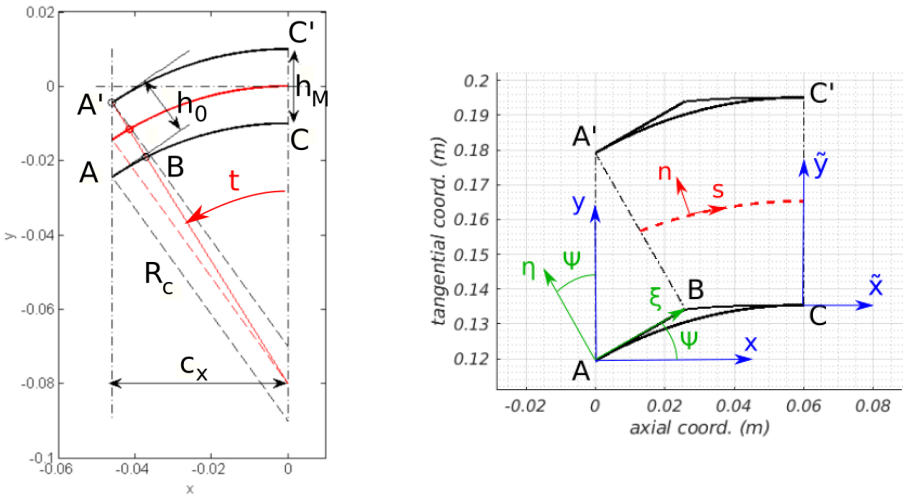

(a) (b)

Fig. 2 Radial cut showing vane mean camber (a) and the inter-vane channel with the modified vanes profile used in the mode-matching problem statement (b). (Fig. (a) taken from Roger *et al.* [2])

To derive the solution of the velocity potentials inside the cambered part of the inter-vane channels (from the BA' interface to the channel outlet CC' in Fig. 2b), two effects need to be addressed : the curvature of the channel centerline and the stream-wise variation of the cross-section (diffuser effect). In a first approach, the centerline curvature was not included in the mode-matching technique [2, 5, 6] because i) its impact on sound transmission phenomena has been considered of secondary importance compared to the diffuser effect and ii) this hypothesis ensures faster computations. In that case, the velocity potentials were given by Rienstra's [9] linearized slowly-varying solution, based on a multiple-scale analysis. This formulation provides closed-form expressions for sound transmission through the OGV row. The model proved to perform well in some cases [6] but showed limitations when increasing frequency. At higher frequencies, the effect of curvature can no longer be neglected. Assuming a slowly-varying curvature, Brambley & Peake [10] developed an extension of Rienstra's work [9] including the effects of curvature. This solution can be implemented to compute the velocity potentials in the inter-vane channels. Both Rienstra [9] and Brambley & Peake's [10] formulations are tested in this paper. The following section describes how these solutions are implemented in the mode-matching technique of Roger *et al.* [2] and gives all needed velocity potential formulations and matching equations.

B. Matching Equations

1. Conservation Laws for Axial-Flow Rotor-Stator Stages

The basic equations that need to be satisfied through the OGV row are the conservation of mass and the conservation of total enthalpy. Assuming an inviscid perfect isentropic irrotational gas flow and harmonic fluctuations, Bouley *et al.* [1] showed that the aforementioned conservation laws reduce to the continuity of fluctuating pressure p' and

fluctuating axial velocity u'_x written as

$$p' = i\rho_0 k c_0 \phi + \mathbf{U_0} \cdot \boldsymbol{\nabla}\phi,$$
$$u'_x = \frac{\partial \phi}{\partial x},$$

in which k is the acoustic wavenumber and ρ_0, c_0 and $\mathbf{U_0}$ are the mean fluid density, sound speed and velocity. Finally, without mean flow, the continuity equations simply concern the velocity potential ϕ and its gradient $\partial\phi/\partial x$. Two sets of equations are then written at the leading-edge ($x = 0$) and the trailing-edge ($x = c_x$) interfaces. The velocity potential and its gradient are gathered into a vector Γ_γ. The index γ stands either for the incident (i), reflected (r) or transmitted (t) waves, or for the downstream (d) and upstream (u) acoustic waves inside the channels

$$\Gamma_\gamma(x, y) = \begin{pmatrix} \phi_\gamma \\ \partial\phi_\gamma/\partial x \end{pmatrix}, \quad \gamma = i, r, t, d, u.$$

The matching equations for the leading-edge (LE) and trailing-edge (TE) interfaces then read

$$\begin{cases} \Gamma_i + \Gamma_r = \Gamma_d + \Gamma_u & \text{at LE,} \\ \Gamma_d + \Gamma_u = \Gamma_t & \text{at TE.} \end{cases} \tag{1}$$

These equations can be directly rewritten on the acoustic modal coefficients. The related developments are described in the following sections.

2. Leading-Edge Interface

Matching equations at the leading-edge interface involve the incident wave ϕ_i, the scattered reflected ϕ_r and transmitted ϕ_d waves. The velocity potential ϕ_u generated from trailing-edge scattering will be added in section II.B.4. Since the inter-vane channel is staggered by an angle Ψ, the transmitted ϕ_d velocity potential is written in the channel system of coordinates (ξ,η) shown in Fig. 2b. With the modal function for a straight duct of constant height being $\psi_q(\eta) = \cos(\alpha_q \eta)$, the potentials read

$$\phi_i(x, y) = \mathrm{e}^{i\alpha_j y}\mathrm{e}^{ik_j^+ x}, \quad \phi_r(x, y) = \sum_{p=-\infty}^{+\infty} R_p \mathrm{e}^{i\alpha_p y}\mathrm{e}^{ik_p^- x}, \quad \phi_d(\xi, \eta) = \sum_{q=0}^{+\infty} D_q \psi_q(\eta)\mathrm{e}^{ik_q^+ \xi},$$

where α_j, α_p, α_q, k_j, k_p and k_q are the transverse and axial wavenumbers defined by

$$\alpha_j = \frac{j}{R_0}, \quad \alpha_p = \alpha_j + p\frac{2\pi}{h_M}, \quad \alpha_q = \frac{q\pi}{h_0} \quad \text{and} \quad k_\zeta^\pm = \pm\sqrt{k^2 - \alpha_\zeta^2}, \quad \zeta = j, p, q.$$

Indices $(j, p) \in \mathbb{Z}^2$ are the azimuthal modal orders of the incident and reflected waves respectively and $q \in \mathbb{N}^*$ is the order of the inter-vane channel mode. R_0 is the radius of the cut through the OGV row.

From Roger *et al.* [2], the matching equations at the leading-edge interface (1) can be recast to yield a first equation (2) on the modal coefficients D_q of the transmitted channel modes and a second one on the reflected modes coefficients R_p (3), as

$$\sum_{q=0}^{+\infty} D_q \varphi_{q,p}^+ \left(k_p^- - \mathcal{K}_{q,p}^+\right) = h_M \left(k_p^- - k_j^+\right) \delta_{p,0}, \tag{2}$$

$$R_p = \frac{1}{h_M} \sum_{q=0}^{+\infty} D_q \varphi_{q,p}^+ - \delta_{p,0}, \tag{3}$$

with

$$\varphi_{q,p}^\pm(\Psi) = \begin{cases} \dfrac{-iu_{q,p}^\pm(\Psi)}{(q\pi/h_M)^2 - u_{q,p}^{\pm 2}(\Psi)} \left(1 - (-1)^q e^{ih_M u_{q,p}^\pm(\Psi)}\right), \\ \dfrac{h_M}{2}(1 + \delta_{q,0}) \quad \text{if} \quad \left|u_{q,p}^\pm(\Psi)\right| = \dfrac{q\pi}{h_M}, \end{cases} \qquad \delta_{q,0} = \begin{cases} 1 & \text{if} \quad q = 0, \\ 0 & \text{otherwise,} \end{cases}$$

$$\mathcal{K}_{q,p}^\pm = k_q^\pm \cos\Psi - \left(\frac{q\pi}{h_M}\right)^2 \frac{\tan\Psi}{u_{q,p}^\pm(\Psi)}, \quad u_{q,p}^\pm(\Psi) = k_q^\pm \sin\Psi - \alpha_p.$$

3. Trailing-Edge Interface

At the trailing-edge interface the downstream wave ϕ_d is scattered into a reflected upstream wave ϕ_u in the channel and a transmitted wave ϕ_t downstream of the OGV row. The channel velocity potentials ϕ_d and ϕ_u are now expressed in terms of a curvilinear abscissa s, varying from 0 at the inlet (BA') to L_c at the outlet (CC'), and its associated curvilinear ordinate $n(s)$ represented in Fig. 2b. The cross-height $h(s)$ varies from h_0 at the inlet (BA') to h_M at the outlet (CC'). The velocity potentials ϕ_d and ϕ_u can be expressed using either Rienstra's solution [9] if the curvature is neglected or Brambley & Peake's solution [10] otherwise. The transmitted potential ϕ_t is expressed in its local system of coordinates $(\tilde{x},\tilde{y})$ linked to (x,y) by $\tilde{x} = x - c_x$ and $\tilde{y} = y - R_c(1-\cos\Psi)$. This gives (details are provided in Appendix A)

$$\phi_d(s,n) = \sum_{q=0}^{+\infty} D_q \mathrm{e}^{ik_q^+ h_M \sin\Psi} \sum_{\nu=0}^{+\infty} B_\nu^q(0) \frac{\Upsilon_\nu^+(s)}{\Upsilon_\nu^+(0)} \sum_{\mu=0}^{+\infty} A_\mu^\nu(s) \psi_\mu^*(s,n),$$

$$\phi_u(s,n) = \sum_{q=0}^{+\infty} U_q \sum_{\nu=0}^{+\infty} B_\nu^q(L_c) \frac{\Upsilon_\nu^-(s)}{\Upsilon_\nu^-(L_c)} \sum_{\mu=0}^{+\infty} A_\mu^\nu(s) \psi_\mu^*(s,n) \quad \text{and} \quad \phi_t(\tilde{x},\tilde{y}) = \sum_{p=-\infty}^{+\infty} R_p \mathrm{e}^{i\alpha_p \tilde{y}} \mathrm{e}^{ik_p^+ \tilde{x}},$$

where the star symbol $*$ denotes modal functions and wavenumbers of the slowly-varying part of the channel. The coefficients A_μ^q, B_ν^q, the modal function ψ_q^* and the modal amplitude variation $\Upsilon_q^\pm$ are computed differently in the cases of Rienstra [9] and Brambley & Peake [10].

When using Rienstra's solution, $A_\mu^q = \delta_{\mu,q}$, $B_\nu^q = \delta_{\nu,q}$, and

$$\psi_q^*(s,n) = \cos\left(\alpha_q^*(s)\left[n + \frac{h(s)}{2}\right]\right), \quad \Upsilon_q^\pm(s) = \frac{\exp\left(i\int_{s_0}^s k_q^{\pm *}\,\mathrm{d}s'\right)}{\left(\rho_0 k_q^{\pm *}\right)^{1/2}} \quad \text{with} \quad s_0 = \begin{cases} 0 & \text{for } \Upsilon_q^+, \\ L_c & \text{for } \Upsilon_q^-, \end{cases}$$

while the wavenumbers are given by

$$\alpha_q^*(s) = q\pi/h(s) \quad \text{and} \quad k_q^{\pm *}(s) = \pm\sqrt{k^2 - \alpha_q^{*2}(s)}.$$

If Brambley & Peake's solution is used instead, the modal shape $\tilde{\psi}_q$ and the axial wavenumber are computed numerically using a Chebyshev collocation method [10]. Since the modal basis varies from the leading-edge interface to the trailing-edge interface, a projection is needed and coefficients A_μ^q and B_ν^q are computed as

$$\tilde{\psi}_q(s,n) = \sum_{\mu=0}^{+\infty} A_\mu^q(s) \psi_\mu^*(s,n) \quad \text{and} \quad \psi_q^*(s,n) = \sum_{\nu=0}^{+\infty} B_\nu^q(s) \tilde{\psi}_\nu(s,n).$$

The modal amplitude variation $\Upsilon_q^\pm$ is also changed to

$$\Upsilon_q^\pm(s) = \frac{\exp\left(i\int_{s_0}^s k_q^{\pm *}\,\mathrm{d}s'\right)}{\left(\rho_0 k_q^{\pm *} \int_{-h(s)/2}^{h(s)/2} \tilde{\psi}_q^2/(1-\kappa n)\,\mathrm{d}n\right)^{1/2}},$$

in which κ is the channel centerline curvature. In Brambley & Peake's formulation [10], $\tilde{\psi}_q$ is normalized so that the integral of $\tilde{\psi}_q^2$ over the cross-height is equal to one. Hence, this solution generalizes Rienstra's solution [9] given that the modal shapes and wavenumbers computed numerically converge toward the analytical solution as κ tends to zero.

Using the continuity equations at the trailing-edge interface (1) gives the equations on both sets of reflected U_q and transmitted T_p modal coefficients as

$$\sum_{q=0}^{+\infty} U_q (k_p^+ - k_q^{-*}(L_c)) \varphi_{q,p}^0 = \sum_{q=0}^{+\infty} D_q \mathrm{e}^{ik_q^+ h_M \sin\Psi} \sum_{\nu=0}^{+\infty} B_\nu^q(0) \frac{\Upsilon_\nu^+(L_c)}{\Upsilon_\nu^+(0)} (k_\nu^{+*}(L_c) - k_p^+) \sum_{\mu=0}^{+\infty} A_\mu^\nu(L_c) \varphi_{\mu,p}^0, \tag{4}$$

$$T_p = \frac{1}{h_M}\left(\sum_{q=0}^{+\infty} D_q \mathrm{e}^{ik_q^+ h_M \sin\Psi} \sum_{\nu=0}^{+\infty} B_\nu^q(0) \frac{\Upsilon_\nu^+(L_c)}{\Upsilon_\nu^+(0)} \sum_{\mu=0}^{+\infty} A_\mu^\nu(L_c) \varphi_{\mu,p}^0 + U_q \varphi_{q,p}^0\right), \tag{5}$$

The projection function $\varphi_{q,p}^0 = \varphi_{q,p}^\pm(\Psi = 0)$ stands for the particular case of a zero-stagger interface, such as the trailing-edge interface for an OGV row.

4. Iterative Procedure

The mode-matching technique runs an iterative procedure of leading-edge/trailing-edge matchings until a converged solution on modal coefficients is reached. At the beginning only the incident wave ϕ_i is known. At the first iteration, the leading-edge matching equations (2) and (3) are solved to get D_q and R_p. The modal coefficients D_q are then used to compute the trailing-edge matching equations (4) and (5), giving U_q and T_p. At the following iterations, the modified leading-edge matching equations (6) and (7), taking into account the reflected channel wave ϕ_u, are solved. Then the same trailing-edge matching equations (4) and (5) as for the first iteration are used. This iterative procedure ends when modal coefficients are considered converged, i.e when the difference in acoustic power between two consecutive iterations is sufficiently low.

The modified equations at the leading-edge interface are

$$\sum_{q=0}^{+\infty} D_q \left(k_p^- - \mathcal{K}_{q,p}^+\right) \varphi_{q,p}^+ = h_M \left(k_p^- - k_j^+\right) \delta_{p,0} + \sum_{q=0}^{+\infty} U_q \sum_{\nu=0}^{+\infty} B_\nu^q(L_c) \frac{\Upsilon_\nu^-(0)}{\Upsilon_\nu^-(L_c)} \sum_{\mu=0}^{+\infty} A_\mu^\nu(0) \left(\mathcal{K}_{\mu,p}^- - k_p^-\right) \varphi_{\mu,p}^- \mathrm{e}^{-ik_\mu^- h_M \sin\Psi}, \tag{6}$$

and

$$R_p = \frac{1}{h_M} \left(\sum_{q=0}^{+\infty} D_q \varphi_{q,p}^+ + U_q \sum_{\nu=0}^{+\infty} B_\nu^q(L_c) \frac{\Upsilon_\nu^-(0)}{\Upsilon_\nu^-(L_c)} \sum_{\mu=0}^{+\infty} A_\mu^\nu(0) \varphi_{\mu,p}^- \mathrm{e}^{-ik_\mu^- h_M \sin\Psi} \right) - \delta_{p,0}, \tag{7}$$

III. Comparison With Numerical Simulations

A. Methodology

A couple of test cases have been defined to test the present analytical solution against numerical simulations computed with the commercial software Simcenter 3D Acoustics [11]. The two-dimensional Helmholtz problem is addressed using a high-order adaptive Finite Element Method (FEM) [12, 13]. Periodic boundary conditions are enforced and the far-field reflections are avoided using Perfectly Matched Layers (PML) [14] as shown in Fig. 3. Qualitative and quantitative comparisons in terms of real values of fluctuating pressure between FEM results and the mode-matching technique are presented below.

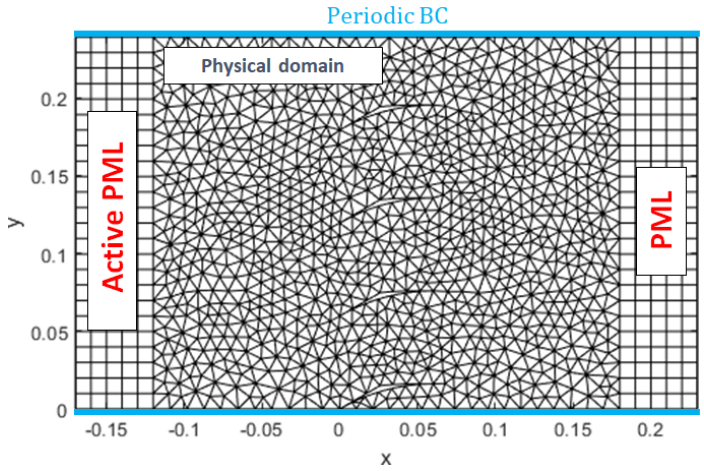

Fig. 3 Explanatory scheme of the numerical setup showing how boundary conditions are treated.

B. Results

1. Vane Camber Effect

Four vanes ($V = 4$) are taken at a duct radius of $R_0 = 38$ mm, with a leading-edge camber angle $\Psi = 30°$ and an axial chord length $c_x = 60$ mm. No mean flow is considered ($M = 0$) and the mean density and sound speed are

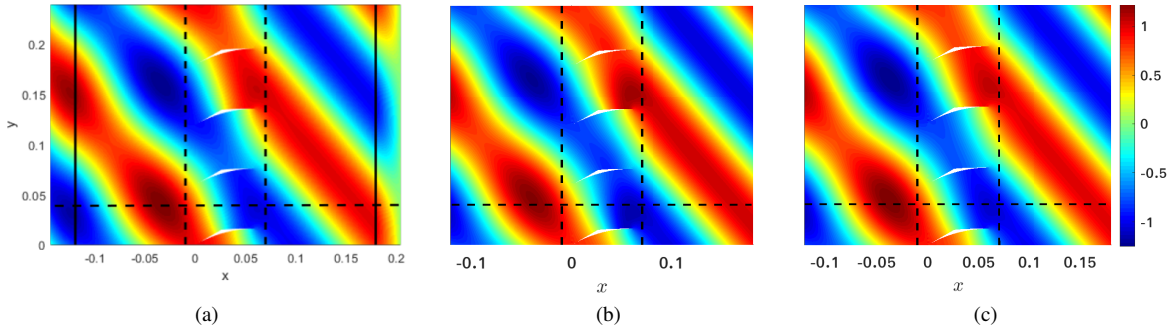

Fig. 4 Instantaneous pressure maps computed with FEM (a), Mode-Matching without camber (b) and Mode-Matching with camber (c) for $j = 1$ and $kc_x = 2.44$. Dashed black lines are the locations for quantitative comparisons and solid black lines in Fig. 4a show the limit of PML.

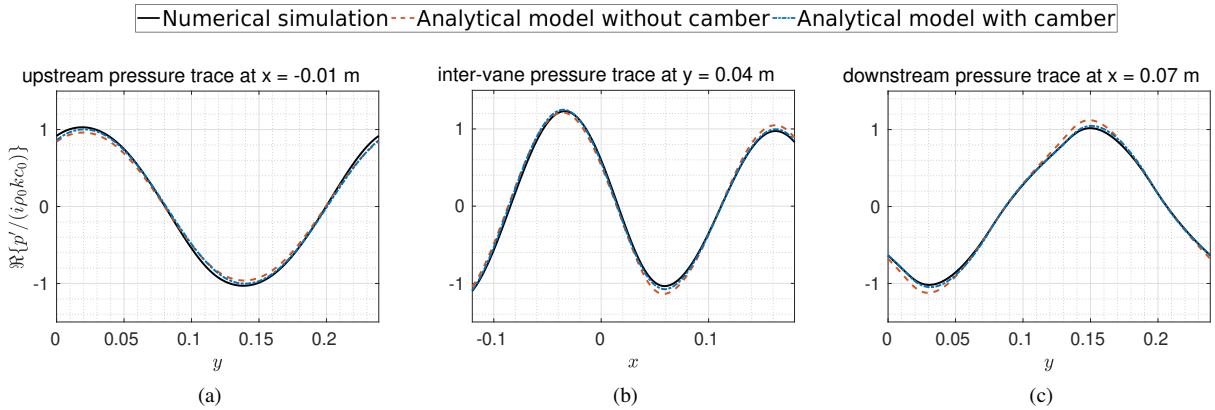

Fig. 5 Comparison of instantaneous pressure profiles between FEM and Mode-Matching technique for $j = 1$ and $kc_x = 2.44$ at $x = -0.01$ m (a), $y = 0.04$ m (b) and $x = 0.07$ m (c).

assumed constant and set to $\rho_0 = 1.225$ kg/m^3 and $c_0 = 340$ m/s. Incident acoustic waves of unit amplitude are scattered by the OGV. Computations have been performed for two distinct incident mode orders, $j = 1$ at $kc_x = 2.44$ ($f \simeq 2200$ Hz) and $j = 5$ at $kc_x = 12.2$ ($f \simeq 11000$ Hz), with corresponding angles of incidence from the x-direction given by $\theta_j = \arcsin(j/kR_0)$ to ensure periodicity in the y-direction.

Figure 4 shows the instantaneous pressure maps computed with the FEM code and the mode-matching technique at $j = 1$ and $kc_x = 2.44$. The pressure patterns are in good agreement upstream and downstream the OGV row, as well as in the inter-vane channels, for both analytical models with and without camber effects. Figure 5 shows the instantaneous pressure profiles extracted upstream, downstream and through the OGV row as shown in dashed black lines in Fig. 4. These quantitative results comfort the conclusion that the model based on Rienstra's solution [9] performs well at low frequencies even without accounting for vane curvature. Yet accounting explicitly for the curvature produces a better match with the numerical solution.

When increasing the frequency to $kc_x = 12.2$ and changing the incident mode order to $j = 5$, the same fairly good agreement is still observed upstream (Fig. 7a). However the simplified model displays significant discrepancies beyond $x = 2c_x/3$ compared to the numerical simulation (Fig. 7b). These differences are also observable on the downstream profile (Fig. 7c). Including the vane camber using Brambley & Peake's solution [10] then gives much better results (Fig. 6 and Fig. 7). The new model proves to be efficient to predict the pressure pattern evolution inside the inter-vane channels but there are still some differences with FEM results when looking at the downstream pressure profile in Fig. 7c. Work is still in progress to understand the residual errors at high frequencies. The new algorithm already shows promising capabilities at the cost of a reasonably higher computation time. The mode-matching code without camber effects runs in less than 2 seconds for a given frequency while it takes around 17 seconds accounting for vane camber, with a not yet optimized MATLAB code.

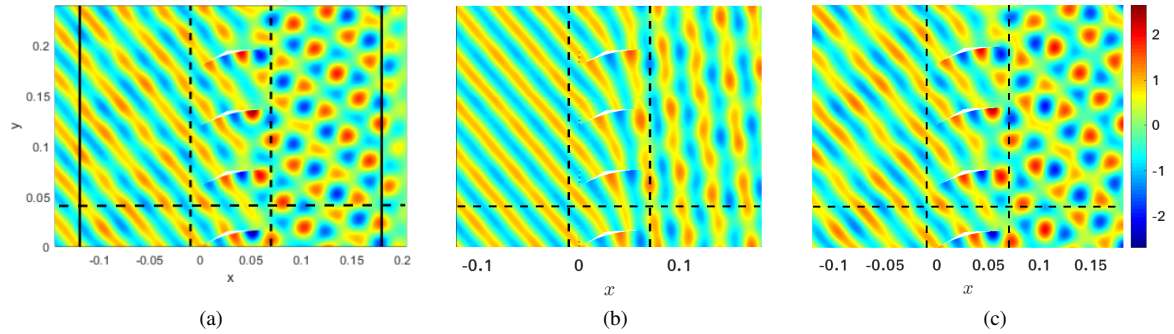

Fig. 6 Instantaneous pressure maps computed with FEM (a), Mode-Matching without camber (b) and Mode-Matching with camber (c) for $j = 5$ and $kc_x = 12.2$. Dashed black lines are the locations for quantitative comparisons and solid black lines in Fig. 6a show the limit of PML.

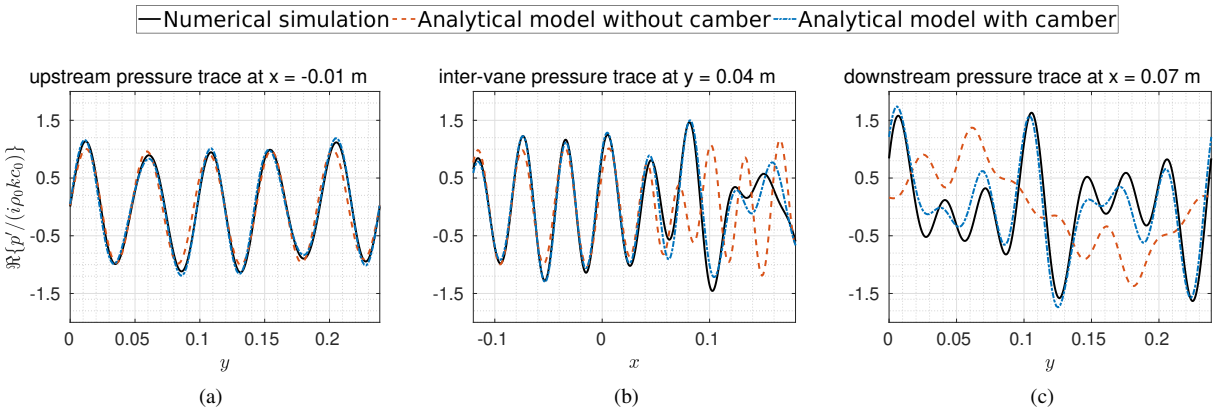

Fig. 7 Comparison of instantaneous pressure profiles between FEM and Mode-Matching technique for $j = 1$ and $kc_x = 2.44$ at $x = -0.01$ m (a), $y = 0.04$ m (b) and $x = 0.07$ m (c).

2. Vane Profile Approximation Effect

In the previous analysis, numerical simulations were performed using the same geometry as in the mode-matching model. In an industrial case of vane row pre-design the vane profile could have thickness and camber varying along the chord. It is therefore important to quantify the effect of the approximated vane geometry to see if a more refined description will be needed for future acoustics predictions. To test this effect, the NASA Source Diagnostic Test (SDT) OGV geometry studied by Hixon [7] has been chosen. The cascade is made of fifty-four vanes ($V = 54$) of chord length $c = 40$ mm taken at a duct radius of $R_0 = 22.35$ cm. Numerical simulations using the real geometry have been carried out to compare the results with those of the mode-matching technique including camber effects and using two different approximated vane geometries (Fig. 8). The camber-angle model uses the same leading-edge camber angle of $\Psi = 33.66°$ to fit the real deviation from the leading edge to the trailing edge. It has therefore a greater stagger angle (16.83°) than the real stagger angle of 11° and a slightly longer chord length $c = 41$ mm. The stagger-angle model has instead the same stagger angle of 11° but a substantially lower leading-edge camber angle ($\Psi = 22°$). No mean flow is considered ($M = 0$) and the mean density and sound speed are constant and set to $\rho_0 = 1.225$ kg/m^3 and $c_0 = 340$ m/s. Computations have been performed for two different incident acoustic waves: mode order $j = 6$ at the frequency $f = 5726$ Hz and mode order $j = -18$ at the frequency $f = 11452$ Hz.

Figures 9 and 10 show the instantaneous pressure fields obtained at $f = 5726$ Hz with the incident mode order $j = 6$. The scattered sound field is well reproduced by the modified circle arc geometry used in the mode-matching technique (Fig. 9) but the approximated vane geometry with the real stagger angle gives slightly better results upstream the OGV row and inside the inter-vane channels than the geometry using the real leading-edge camber angle (Fig. 10a and Fig. 10b). Note that the higher stagger angle in the camber-angle vane model does not have any significant effect on the transmitted sound field at this frequency (Fig. 10c).

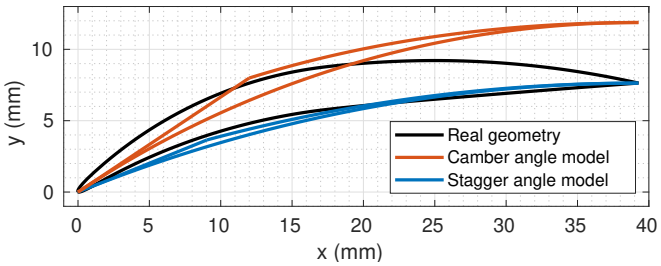

Fig. 8 Approximated vane profiles used in the mode-matching technique compared to the real geometry used in the numerical simulation.

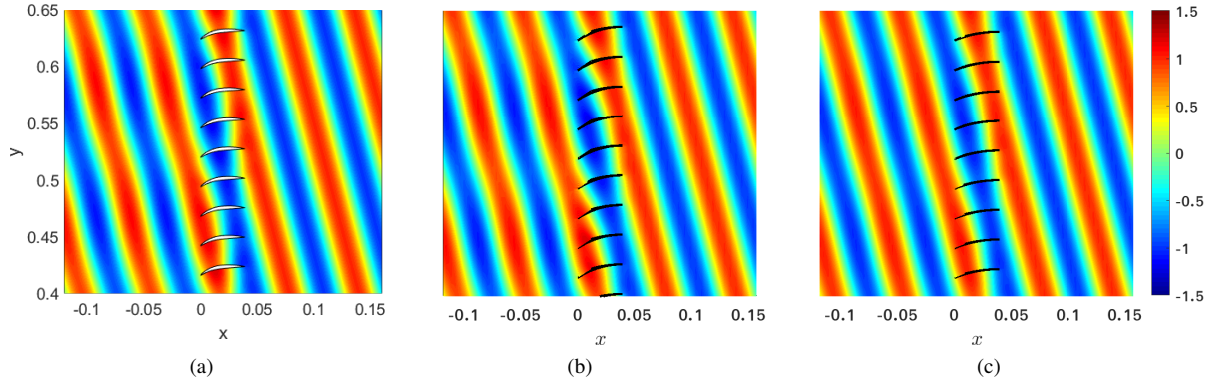

Fig. 9 Instantaneous pressure maps computed with FEM (a), Mode-Matching with the same leading-edge camber angle (b) and Mode-Matching with the same stagger angle (c) for $j = 6$ and $f = 5726$ Hz.

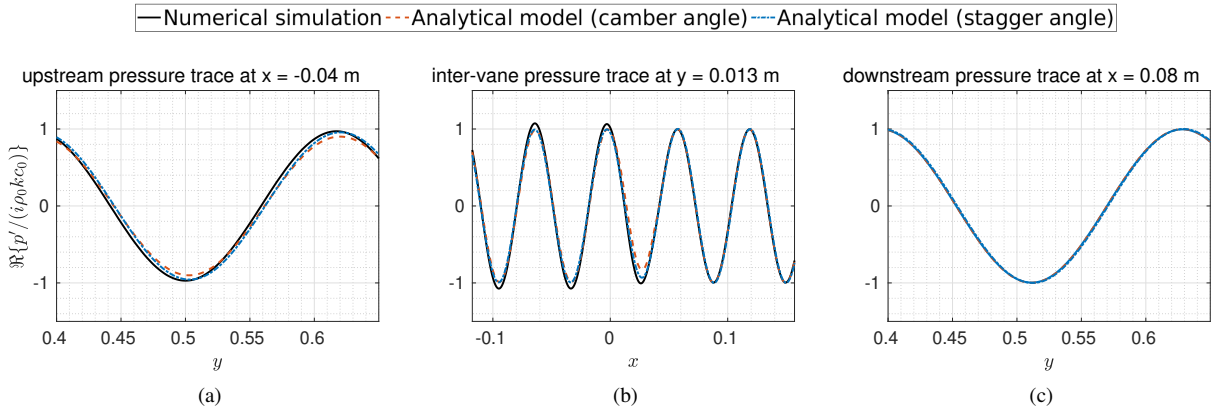

Fig. 10 Comparison of instantaneous pressure profiles between FEM and Mode-Matching technique for $j = 1$ and $kc_x = 2.44$ at $x = -0.04$ m (a), $y = 0.013$ m (b) and $x = 0.08$ m (c).

At the frequency $f = 11452$ Hz, with an incident mode order $j = -18$, discrepancies between the analytical solution and the numerical solution are more significant (Fig. 11 and Fig. 12). These deficiencies are expected since high frequency waves are more sensitive to small details of the vane geometry. Note that the pressure field computed with the camber-angle vane model is in better agreement with the numerical solution in this case, especially upstream the OGV row where the stagger-angle model seems to miss a cut-on reflected mode.

Up to the frequency $f = 11452$ Hz, the modified circle arc geometry is able to generate a pressure field in fairly good agreement with the FEM results. The model using the same leading-edge camber angle should be preferred as it reproduces more precisely the reflected scattered waves.

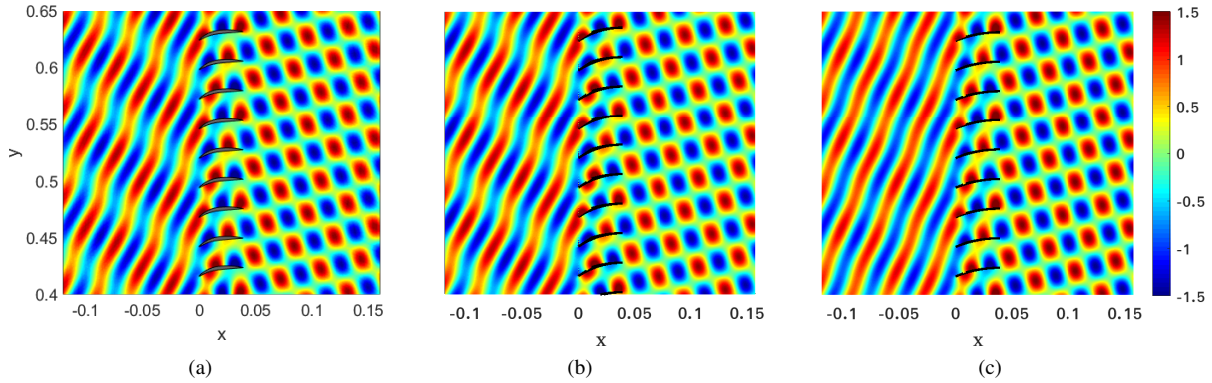

(a) (b) (c)

Fig. 11 Instantaneous pressure maps computed with FEM (a), Mode-Matching with the same leading-edge camber angle (b) and Mode-Matching with the same stagger angle (c) for $j = -18$ and $f = 11452$ Hz.

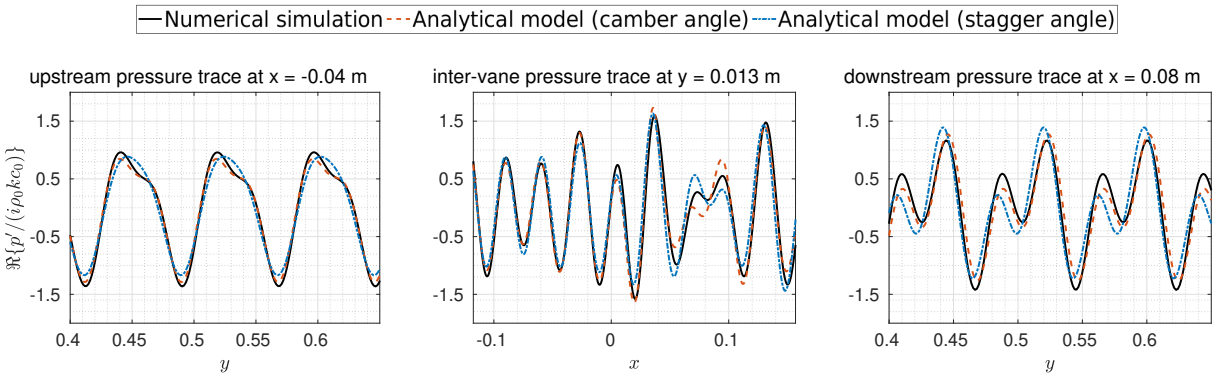

(a) (b) (c)

Fig. 12 Comparison of instantaneous pressure profiles between FEM and Mode-Matching technique for $j = -18$ and $f = 11452$ at $x = -0.04$ m (a), $y = 0.013$ m (b) and $x = 0.08$ m (c).

IV. Inter-Vane Channel Mode Transitions

A. Mode Transition in Ducts of Varying Cross-Section

An important fact when dealing with mode transmission through channels of varying cross-section is the possibility for a cut-on mode to turn cut-off, or vice versa. This phenomenon was highlighted by Rienstra [15]. In the case of a converging duct, an incident cut-on mode undergoing transition would be totally reflected back, leaving only an evanescent mode beyond. Those phenomenons can occur in OGV inter-vane channels showing cross-section variation. In case of such a transition, the wave behavior in the inter-vane channels of an OGV row is changed and there could be a significant influence on the acoustic power balance between the reflected and transmitted powers. Both cut-on/cut-off and cut-off/cut-on transitions and their possible effects on modal energy distribution are highlighted below using a solution derived from Ovenden's work [8] explained in Appendix B. One important underlying hypothesis is the energy conservation of a mode when undergoing transition, avoiding transfer of energy to neighboring modes. Finally, even if the curvature is not accounted for in this preliminary discussion, the transition mechanisms *a priori* remain the same. The implementation of the transitions in Brambley & Peake's [10] solution is presently in progress.

B. Energy Pumping by Acoustic Tunnel Effect

A cut-off mode generated at the leading-edge interface which undergoes transition expectedly has a higher amplitude at the trailing-edge interface than if was simply cut-off, especially if the transition occurs sufficiently close to the leading edge as shown in Fig. 13. Hence, a possibly significant quantity of energy could propagate into the inter-vane channel *via* this mode, generating what is called acoustic energy pumping. This mechanism allows energy transmission from

upstream to downstream that would not occur without cut-off/cut-on transition. It is then expected that acoustic tunnel effect increases the relative part of transmitted power through the OGV. In Fig. 13b, the amplitude variation for a given

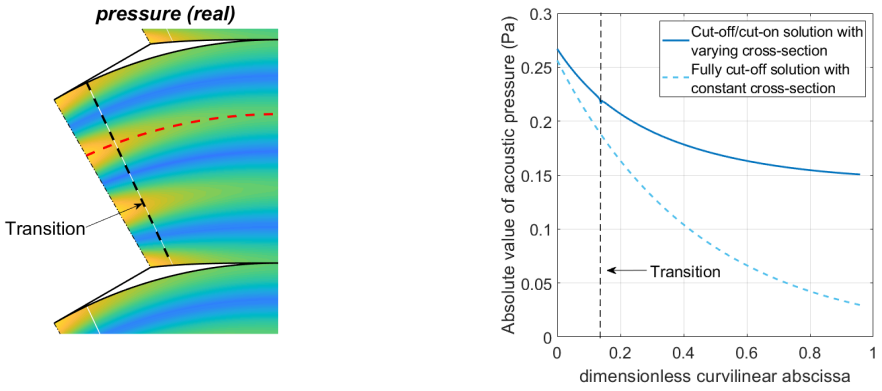

(a) (b)

Fig. 13 (a) Pressure amplitude map of an evanescent mode generated at the leading-edge interface and undergoing cut-off/cut-on transition at 14.6 % of the channel length. (b) Amplitude decay along the red dashed line in Fig. 13a.

curvilinear abscissa plotted in dashed red line in Fig. 13a shows the difference between a cut-off mode which undergoes transition and the equivalent fully cut-off mode computed with a constant cross-height taken at the inlet. The difference before the transition is partially due to the reflection of the cut-off mode where the transition occurs and the variation of the cross-section. Note that the amplitude of the cut-off/cut-on solution is still decaying after the transition but only because the channel cross-section is increasing.

C. Standing Wave Pattern

An upstream propagating mode, generated at the trailing-edge interface, which undergoes transition in the channel will be reflected at the transition location. The upstream propagating mode added to its reflection forms a standing wave pattern. A typical pressure amplitude map can be seen in Fig. 14. The pressure amplitude at the trailing edge location is therefore highly affected by transition. On the other side of the transition, only an evanescent wave is transmitted, which

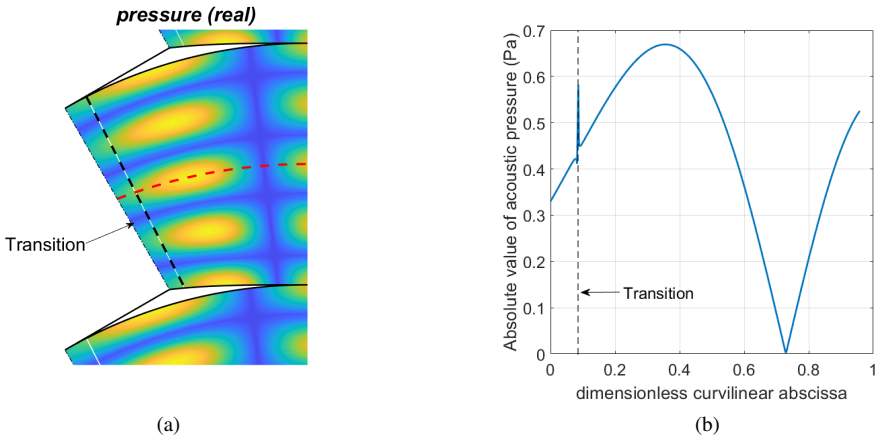

(a) (b)

Fig. 14 (a) Pressure amplitude map of an upstream propagating mode generated at the trailing-edge interface and undergoing cut-on/cut-off transition at 8.8 % of the channel length. (b) Amplitude decay along the red dashed line in Fig. 14a.

substantially reduces the energy transferred upstream of the OGV, especially if the transition occurs far enough from the leading edge.

V. Conclusion

An improved mode-matching model including vane camber for OGV aeroacoustics studies has been developed in this paper. In particular, comparisons with numerical simulations have shown the importance of accounting explicitly for vane camber when modeling sound transmission through vanes row at high frequencies. The improved model still shows residual discrepancies with numerical simulations in the transmitted field. This is under investigation to further improve the current model, looking at possible curvature-gradient effects. Only a reasonably higher computation time is needed to account for vane camber with a non optimized MATLAB code, which makes the model attractive for broadband-noise predictions. However, the simplified model without camber should be preferred for predictions at low frequencies since it has proved accuracy in this range.

Encouraging results have been obtained with the mode-matching model compared to numerical simulations using a more realistic vane geometry. Even if more discrepancies can be expected at higher frequencies than presented in this paper, the model proves to give accurate results hence a more refined vane geometry description is not necessary in this range. Results with a mean potential flow have also been performed in Moreau *et al.* [16], using the simplified mode-matching model, and give a reasonably good match with numerical simulations carried out using the Simcenter 3D Acoustics software.

The formalism used in the mode-matching technique is also well suited to implement cut-off/cut-on and cut-on/cut-off transitions in the inter-vane channels. These transitions have already been implemented in the mode-matching technique without camber, with a uniformly valid solution derived from Rienstra [15] and Ovenden's work [8]. Ongoing derivations will allow the addition of transitions when also accounting for curvature [10]. It could be argued that the effect of those transitions on broadband noise could be negligible at low and medium frequencies since only few and relatively small frequency ranges would be significantly affected. At high frequencies though, these frequency ranges become wider and several modes can undergo transition at the same frequency. A greater effect may be expected then but this needs to be confirmed quantitatively. Furthermore, the selective modal content of tonal noise in turbomachines could be more sensitive to the occurrence of transitions. One limitation in the present solutions [8, 10, 15] could be that the energy conservation of a cut-on mode prevents it from transferring energy to neighboring modes at a transition. Ovenden *et al.* [17] have presented FEM results showing examples of modes transferring a significant amount of energy to neighboring modes when undergoing transition. They found that such modal scattering may be expected when both the radial mode order and the frequency are high enough in slowly-varying cylindrical ducts. Smith *et al.* [18] then studied flow and geometry induced scattering when a transition occurs at such high frequencies. Their work could be implemented in the current mode-matching technique if deemed necessary. Otherwise, the multimodal approach of Felix & Pagneux [19] could also be used but it would substantially increase the computation time.

Other developments presently in progress include the implementation of a Kutta condition in the mode-matching formulation with vane camber. Then the next objective is to model sound generation from impinging wakes at the leading edge.

A. Matching Constant and Slowly Varying Velocity Potential Formulations

A. Potentials without Curvature

The potential $\phi_d(s,n)$ of the wave propagating downstream from the leading edge is expressed from Rienstra [9, 15] as

$$\phi_d(s,n) = \sum_{q=0}^{+\infty} Q_{q,d}\psi_q^*(s,n)\Upsilon_q^+(s).$$

In the constant cross-section part of the channel, from the leading-edge interface AA' to the interface BA', the same mode is given by

$$\phi_d(\xi,\eta) = \sum_{q=0}^{+\infty} D_q\psi_q(\eta)\mathrm{e}^{ik_q^+\xi}.$$

At the BA' interface, the systems of coordinates are

$$\begin{cases} s = 0, \\ n = \eta - h_0/2 \end{cases} \quad \text{and} \quad \begin{cases} \xi = h_M \sin\Psi, \\ \eta \in [0, h_0]. \end{cases}$$

Hence $\psi_q^*(s=0,n) = \psi_q(\eta)$ and matching the two solutions gives

$$Q_{q,d} = D_q \frac{\mathrm{e}^{ik_q^+ h_M \sin\Psi}}{\Upsilon_q^+(0)},$$

so that the velocity potential in the slowly-varying part is recast to

$$\phi_d(s,n) = \sum_{q=0}^{+\infty} D_q \psi_q^*(s,n) \frac{\Upsilon_q^+(s)}{\Upsilon_q^+(0)} \mathrm{e}^{ik_q^+ h_M \sin\Psi}. \tag{8}$$

Scattering at the trailing-edge interface generates reflected modes $\phi_u(s,n)$ in the slowly varying part of the inter-vane channels. The solution is expressed from Rienstra [9, 15] as

$$\phi_u(s,n) = \sum_{q=0}^{+\infty} \tilde{Q}_{q,u} \psi_q^*(s,n) \Upsilon_q^-(s).$$

For easier integration in the mode-matching technique, a modification is needed to match cosine modes generated at the trailing-edge interface

$$\phi_u(\tilde{x},\tilde{y}) = \sum_{q=0}^{+\infty} U_q \psi_q(\tilde{y}) \mathrm{e}^{ik_q^- \tilde{x}}.$$

At the trailing-edge interface, the systems of coordinates are

$$\begin{cases} s = L_c, \\ n = \tilde{y} - h_M/2 \end{cases} \quad \text{and} \quad \begin{cases} \tilde{x} = 0, \\ \tilde{y} \in [0, h_M]. \end{cases}$$

Hence $\psi_q^*(s=L_c,n) = \psi_q(\tilde{y})$ and matching the two solutions gives

$$\tilde{Q}_{q,u} = U_q \frac{1}{\Upsilon_q^-(L_c)}.$$

Then, in the constant part of the channel, the reflected modes are given by

$$\phi_u(\xi,\eta) = \sum_{q=0}^{+\infty} Q_{q,u} \psi_q(\eta) \mathrm{e}^{ik_q^-(\xi - h_M \sin\Psi)},$$

and matching at the BA' interface yields

$$Q_{q,u} = U_q \frac{\Upsilon_q^-(0)}{\Upsilon_q^-(L_c)}.$$

Finally, the reflected modes in the constant part of the inter-vane channels are written as

$$\phi_u(\xi,\eta) = \sum_{q=0}^{+\infty} U_q \psi_q(\eta) \frac{\Upsilon_q^-(0)}{\Upsilon_q^-(L_c)} \mathrm{e}^{ik_q^-(\xi - h_M \sin\Psi)}. \tag{9}$$

B. Potentials with Curvature

In the case of Brambley & Peake's solution [10] including curvature, a projection has to be made at the BA' interface to change from the straight modal basis $\left(\psi_q^*\right)_{q\in\mathbb{N}^*}$ to the curved modal basis $\left(\tilde{\psi}_q\right)_{q\in\mathbb{N}^*}$. The projection coefficients are defined as

$$\tilde{\psi}_q(s,n) = \sum_{\mu=0}^{+\infty} A_\mu^q(s)\psi_\mu^*(s,n) \quad \text{and} \quad \psi_q^*(s,n) = \sum_{\nu=0}^{+\infty} B_\nu^q(s)\tilde{\psi}_\nu(s,n),$$

where ψ_q^* is a generalized form of ψ_q accounting for slow variations of the cross-section. Hence a cosine mode $\phi_{d,q}$ of order q propagating downstream from the leading-edge interface is expressed in the slowly varying curved passage as a sum of curved modes

$$\phi_{d,q}(s,n) = D_q \mathrm{e}^{ik_q^+ h_M \sin\Psi} \sum_{\nu=0}^{+\infty} B_\nu^q(0)\tilde{\psi}_\nu(s,n)\frac{\Upsilon_\nu^+(s)}{\Upsilon_\nu^+(0)}.$$

In order to simplify the implementation in the mode-matching technique, a solution in the form of a sum of cosine modal functions is sought. This, and summing on all modes q, yields

$$\phi_d(s,n) = \sum_{q=0}^{+\infty} D_q \mathrm{e}^{ik_q^+ h_M \sin\Psi} \sum_{\nu=0}^{+\infty} B_\nu^q(0)\frac{\Upsilon_\nu^+(s)}{\Upsilon_\nu^+(0)} \sum_{\mu=0}^{+\infty} A_\mu^\nu(s)\psi_\mu^*(s,n). \tag{10}$$

It is possible to describe the reflected waves following the same methodology. A given cosine mode of order q propagating upstream is then expressed in the slowly varying curved passage as a sum of curved modes

$$\phi_{u,q}(s,n) = U_q \sum_{\nu=0}^{+\infty} B_\nu^q(L_c)\tilde{\psi}_\nu(s,n)\frac{\Upsilon_\nu^-(s)}{\Upsilon_\nu^-(L_c)}.$$

The expression in the constant part of the inter-vane channels is then, summing on all modes q

$$\phi_u(\xi,\eta) = \sum_{q=0}^{+\infty} U_q \sum_{\nu=0}^{+\infty} B_\nu^q(L_c)\frac{\Upsilon_\nu^-(0)}{\Upsilon_\nu^-(L_c)} \sum_{\mu=0}^{+\infty} A_\mu^\nu(s)\psi_\mu(\eta)\mathrm{e}^{ik_\mu^-(\xi-h_M\sin\Psi)}. \tag{11}$$

As mentioned in the core text, the formalism for curved ducts of Brambley & Peake [10] is an extension of the straight-duct formalism of Rienstra [9] given that the modal shape functions and axial wavenumbers computed numerically converge to the straight-duct analytical solution when the curvature tends to zero in the Chebyshev collocation solver. In this case the projection coefficients become $A_\mu^q(s) = \delta_{\mu,q}$ and $B_\nu^q(s) = \delta_{\nu,q}$, $\forall s$, and the formulations (10) and (11) become exactly equivalent to (8) and (9).

B. Uniformly Valid Solution with Transition

As shown by Rienstra [15], a transition is a singularity in the linearized slowly varying solution. Since transitions can occur close to a matching interface, a regularized solution as proposed by Ovenden [8, 17] is needed to avoid wrong values of potentials at matching interfaces that would lead to erroneous modal coefficients. For sound propagation inside inter-vane channels, both cut-on/cut-off and cut-off/cut-on transitions are possible. A solution for the velocity potential of a given mode of order q is then proposed that can be used for both transition phenomena. In the inter-vane channel reference frame (S,n), where $S = \epsilon s$ is the slow variable, the expression reads

$$\begin{aligned}\hat{\phi} =& Q\frac{2\sqrt{\pi}e^{i\pi/4}}{\sqrt{\rho_0 k}}\psi_q^*(n;S)\left(\frac{3}{2\epsilon}\frac{1}{\sigma_q^3}\int_{S_t}^{S}\frac{k\sigma_q}{\beta^2}\,\mathrm{d}S'\right)^{1/6}\exp\left(\frac{i}{\epsilon}\int_{S_t}^{S}\frac{kM}{\beta^2}\,\mathrm{d}S'\right)\\ &\times\left[(I_u-\frac{i}{2}I_d)\mathrm{A_i}\left\{\left(-\frac{3i}{2\epsilon}\int_{S_t}^{S}\frac{k\sigma_q}{\beta^2}\,\mathrm{d}S'\right)^{2/3}\right\}+\frac{1}{2}I_d\mathrm{B_i}\left\{\left(-\frac{3i}{2\epsilon}\int_{S_t}^{S}\frac{k\sigma_q}{\beta^2}\,\mathrm{d}S'\right)^{2/3}\right\}\right],\end{aligned} \tag{12}$$

where

$Q =$ constant to be set with a known value of the potential at some point,
$\sigma =$ propagated part of the axial wavenumber,

M = Mach number,
β = $\sqrt{1-M^2}$, Prandtl-Glauert factor,
S_t = transition location.

A_i and B_i are the Airy functions of the first and second kinds. I_d and I_u represent the relative initial amplitudes of the downstream cut-off mode and of the upstream cut-on mode respectively. To use this solution in the leading-edge problem of section IV.B, so for a cut-off mode coming from the left-side of the transition, I_d is set to 1 and I_u to 0 since there is no reflected upstream mode coming from the right-side. This yields

$$\hat{\phi}_{off/on} = Q\frac{\sqrt{\pi}e^{i\pi/4}}{\sqrt{\rho_0 k}}\psi_q^*(n;S)\left(\frac{3}{2\epsilon}\frac{1}{\sigma_q^3}\int_{S_t}^{S}\frac{k\sigma_q}{\beta^2}\,\mathrm{d}S'\right)^{1/6}\exp\left(\frac{i}{\epsilon}\int_{S_t}^{S}\frac{kM}{\beta^2}\,\mathrm{d}S'\right)F_{BA}\left\{\chi(S)\right\},$$

where $F_{BA} \equiv B_i - iA_i$. In the case of section IV.C, for a cut-on mode traveling upward from the trailing-edge interface, I_u is set to 1 and I_d to 0. The solution then reads

$$\hat{\phi}_{on/off} = Q\frac{2\sqrt{\pi}e^{i\pi/4}}{\sqrt{\rho_0 k}}\psi_q^*(n;S)\left(\frac{3}{2\epsilon}\frac{1}{\sigma_q^3}\int_{S_t}^{S}\frac{k\sigma_q}{\beta^2}\,\mathrm{d}S'\right)^{1/6}\exp\left(\frac{i}{\epsilon}\int_{S_t}^{S}\frac{kM}{\beta^2}\,\mathrm{d}S'\right)A_i\left\{\chi(S)\right\},$$

with

$$\chi(S) = \left(-\frac{3i}{2\epsilon}\int_{S_t}^{S}\frac{k\sigma_q}{\beta^2}\,\mathrm{d}S'\right)^{2/3}.$$

Note that the particular case of a cut-on/cut-off solution is exactly Ovenden's result [8] with a change of coordinate $\tilde{S} \to -S$.

Acknowledgements

This work was performed within the framework of the Labex CeLyA of the Université de Lyon, within the programme 'Investissements d'Avenir' (ANR-10-LABX-0060/ANR-16-IDEX-0005) operated by the French National Research Agency (ANR), and is also partially supported by the industrial Chair ADOPSYS co-financed by Safran Aircraft Engines and the ANR (ANR-13-CHIN-0001-01).

References

[1] Bouley, S., François, B., Roger, M., Posson, H., and Moreau, S., "On a two-dimensional mode-matching technique for sound generation and transmission in axial-flow outlet guide vanes," *Journal of Sound and Vibration*, Vol. 403, 2017, pp. 190 – 213. doi:10.1016/j.jsv.2017.04.031.

[2] Roger, M., François, B., and Bauerheim, M., "Three-Dimensional Modeling of Annular Cascade Trailing-Edge Noise," *22nd AIAA/CEAS Aeroacoustics Conference*, Lyon, France, 2016. doi:10.2514/6.2016-2949.

[3] Whitehead, E. A. N., "The theory of parallel-plate media for microwave lenses," *Proceedings of the IEE - Part III: Radio and Communication Engineering*, Vol. 98, 1951, pp. 133 – 140. doi:10.1049/pi-3.1951.0025.

[4] Mittra, R., and Lee, S.-W., *Analytical techniques in the theory of guided waves*, Macmillan, New York, 1971.

[5] Roger, M., and François, B., "Combined analytical models for sound generation and transmission in cambered axial-flow outlet guide vanes," *European Journal of Mechanics - B/Fluids*, Vol. 61, 2017, pp. 218 – 225. doi:10.1016/j.euromechflu.2016.10.006.

[6] Roger, M., and Moreau, S., "Coupled mode-matching and slowly-varying duct formulations for predicting noise generation and transmission in axial-flow rotor-stator stages," *MUSAF III*, Toulouse, France, 2016. URL `http://musaf2016.onera.fr/content/program`.

[7] Hixon, R., "Computational Aeroacoustics Prediction of Acoustic Transmission Through a Realistic 2D Stator," *17th AIAA/CEAS Aeroacoustics Conference*, Portland, Oregon, 2011. doi:10.2514/6.2016-2949.

[8] Ovenden, N., "A uniformly valid multiple scales solution for cut-on cut-off transition of sound in flow ducts," *Journal of Sound and Vibration*, Vol. 286, No. 1, 2005, pp. 403 – 416. doi:10.1016/j.jsv.2004.12.009.

[9] Rienstra, S. W., "Sound transmission in slowly varying circular and annular lined ducts with flow," *Journal of Fluid Mechanics*, Vol. 380, 1999, pp. 279 – 296. doi:10.1017/S0022112098003607.

[10] Brambley, E. J., and Peake, N., "Sound transmission in strongly curved slowly varying cylindrical ducts with flow," *Journal of Fluid Mechanics*, Vol. 596, 2008, pp. 387 – 412. doi:10.1017/S0022112007009603.

[11] "Simcenter 3D Acoustics," , 2019. URL `https://www.plm.automation.siemens.com/global/en/products/simulation-test/acoustic-simulation.html`.

[12] Bériot, H., Prinn, A., and Gabard, G., "Efficient implementation of high-order finite elements for Helmholtz problems," *Int. J. Numer. Methods Eng.*, Vol. 106, No. 3, 2016, pp. 213–240. doi:10.1002/nme.5172.

[13] Bériot, H., and Gabard, G., "Anisotropic adaptivity of the p-FEM for time-harmonic acoustic wave propagation," *J. Comput. Phys.*, Vol. 378, 2019, pp. 234–256. doi:10.1016/j.jcp.2018.11.013.

[14] Bécache, E., Dhia, A. S. B.-B., and Legendre, G., "Perfectly Matched Layers for the Convected Helmholtz Equation," *SIAM J. Numer. Anal.*, 2006. doi:10.1137/S0036142903420984.

[15] Rienstra, S. W., "Sound propagation in slowly varying lined flow ducts of arbitrary cross-section," *Journal of Fluid Mechanics*, Vol. 495, 2003, pp. 157 – 173. doi:10.1017/S0022112003006050.

[16] Moreau, S., Baddoo, P., Bériot, H., and Roger, M., "Two-Dimensional Sound Transmission in Realistic Turbomachinery Cascade," *25th AIAA/CEAS Aeroacoustics Conference*, Delft, Holland, 2019.

[17] Ovenden, N. C., Eversman, W., and Rienstra, S. W., "Cut-on Cut-off Transition in Flow Ducts: Comparing Multiple-scales and Finite-element Solutions," *10th AIAA/CEAS Aeroacoustics Conference*, Manchester, Great Britain, 2004. doi:10.2514/6.2004-2945.

[18] Smith, A., Ovenden, N., and Bowles, R., "Flow and geometry induced scattering of high frequency acoustic duct modes," *Wave Motion*, Vol. 49, No. 1, 2012, pp. 109 – 124. doi:10.1016/j.wavemoti.2011.07.006.

[19] Felix, S., and Pagneux, V., "Sound propagation in rigid bends: A multimodal approach," *The Journal of the Acoustical Society of America*, Vol. 110, No. 3, 2001, pp. 1329 – 1337. doi:10.1121/1.1391249.